2024

Elucidating Granulocytic Myeloid-Derived Suppressor Cell Heterogeneity During Staphylococcus Aureus Biofilm Infection

Blake P. Bertrand

Cortney E. Heim

Scott A. Koepsell

Tammy Kielian

OXFORD JLB JOURNAL OF LEUKOCYTE BIOLOGY

Journal of Leukocyte Biology, 2024, **115**, 620–632

https://doi.org/10.1093/jleuko/qiad158
Advance access publication 14 December 2023
Article

Elucidating granulocytic myeloid-derived suppressor cell heterogeneity during *Staphylococcus aureus* biofilm infection

Blake P. Bertrand, Cortney E. Heim, Scott A. Koepsell, and Tammy Kielian*

Department of Pathology, Microbiology, and Immunology, University of Nebraska Medical Center, 985900 Nebraska Medical Center, Omaha, NE 68198-5900, United States
*Corresponding author: Department of Pathology, Microbiology, and Immunology, University of Nebraska Medical Center, 985900 Nebraska Medical Center, Omaha, NE 68198-5900. Email: tkielian@unmc.edu

Abstract

Myeloid-derived suppressor cells (MDSCs) are pathologically activated immature myeloid cells with immunosuppressive activity that expand during chronic inflammation, such as cancer and prosthetic joint infection (PJI). Myeloid-derived suppressor cells can be broadly separated into 2 populations based on surface marker expression and function: monocytic myeloid-derived suppressor cells (M-MDSCs) and granulocytic myeloid-derived suppressor cells (G-MDSCs). Granulocytic myeloid-derived suppressor cells are the most abundant leukocyte infiltrate during PJI; however, how this population is maintained in vivo and cellular heterogeneity is currently unknown. In this study, we identified a previously unknown population of Ly6G$^+$Ly6C$^+$F4/80$^+$MHCII$^+$ MDSCs during PJI that displayed immunosuppressive properties ex vivo. We leveraged F4/80 and MHCII expression by these cells for further characterization using cellular indexing of transcriptomes and epitopes by sequencing, which revealed a distinct transcriptomic signature of this population. F4/80$^+$MHCII$^+$ MDSCs displayed gene signatures resembling G-MDSCs, neutrophils, and monocytes but had significantly increased expression of pathways involved in cytokine response/production, inflammatory cell death, and mononuclear cell differentiation. To determine whether F4/80$^+$MHCII$^+$ MDSCs represented an alternate phenotypic state of G-MDSCs, Ly6G$^+$Ly6C$^+$F4/80$^-$MHCII$^-$ G-MDSCs from CD45.1 mice were adoptively transferred into CD45.2 recipients using a mouse model of PJI. A small percentage of transferred G-MDSCs acquired F4/80 and MHCII expression in vivo, suggesting some degree of plasticity in this population. Collectively, these results demonstrate a previously unappreciated phenotype of F4/80$^+$MHCII$^+$ MDSCs during PJI, revealing that a granulocytic-to-monocytic transition can occur during biofilm infection.

Keywords: CITE-seq, G-MDSC, *S. aureus*, Transcriptomics

1. Introduction

Myeloid-derived suppressor cells (MDSCs) are a heterogenous group of immature, anti-inflammatory myeloid cells that accumulate during disease states.[1] Under homeostatic conditions, immature myeloid cells differentiate into mature populations such as macrophages, polymorphonuclear neutrophils (PMNs), and dendritic cells; however, in diseases with prolonged inflammation such as cancer and chronic infection, this differentiation process is disrupted, leading to MDSC accumulation.[1] The current model for MDSC activation involves a 2-signal mechanism where growth factors from chronic inflammation cause the expansion of monocyte and/or granulocyte precursors, which are activated at the site of inflammation by proinflammatory cytokines to acquire a suppressive phenotype.[1,2]

MDSCs have been classified into at least 2 subsets, which are defined based on cell surface marker expression, namely, granulocytic (G-MDSCs or PMN-MDSCs) and monocytic (M-MDSCs).[1,3] These subsets share morphological characteristics with their mature myeloid counterparts, which supports their nomenclature. While each population can inhibit T-cell activation, their mechanisms of suppression differ. For example, G-MDSCs have been reported to utilize reactive oxygen species, peroxynitrate, arginase 1, and prostaglandin E2 production, whereas M-MDSCs are typified by nitric oxide, immunosuppressive cytokines (IL-10 and TGF-β), and PD-L1 expression.[1] In general, G-MDSCs represent the major MDSC population in the setting of cancer and chronic infection.[3–5]

The role of MDSCs during cancer has been extensively studied, where they promote tumor metastasis and angiogenesis.[6] However, MDSC involvement in other pathologies is still being elucidated as there are disease-specific contexts that must be considered that influence effector functions.[7] This is highlighted by the observation that G-MDSCs accumulate in the local tumor environment as well as systemically in the blood and spleen of tumor-bearing mice.[8] This contrasts with *Staphylococcus aureus* biofilm infection, where G-MDSCs accumulate locally at the site of prosthetic joint infection (PJI) but are not expanded in the spleen or blood.[9,10] G-MDSCs comprise >70% of the leukocyte infiltrate at the site of PJI and are the major source of IL-10.[11] Notably, G-MDSC recruitment was significantly reduced in IL-10 knockout (KO) mice during *S. aureus* PJI concomitant with increased monocyte infiltrates, resulting in decreased bacterial burden.[11] This finding suggests that IL-10 may play an indirect role in G-MDSC recruitment during PJI. Furthermore, depletion of G-MDSCs during PJI promoted bacterial clearance, demonstrating the immunosuppressive function of these cells.[9] In addition,

Received: September 14, 2023. **Revised:** November 27, 2023. **Accepted:** November 30, 2023. **Corrected and Typeset:** January 8, 2024

G-MDSCs have been shown to inhibit PMN killing of S. *aureus*[12] and attenuate monocyte/macrophage proinflammatory activity in the setting of S. *aureus* PJI.[9,11]

Because G-MDSCs represent a large percentage of the leukocyte infiltrate during PJI, the question remains as to how this population is sustained in vivo and their degree of heterogeneity. In cancer models, G-MDSCs exhibit short half-lives in vivo and are terminally differentiated.[13] In contrast, M-MDSCs can assume different fates in the tumor microenvironment, including differentiation into tumor-associated macrophages or dendritic cells, or even transitioning into G-MDSCs.[14–18] It is unclear whether this plasticity occurs during infection, since the recruitment and activation factors that MDSCs experience are unique due to bacterial-derived pathogen associated molecular patterns and virulence factors that are not present during cancer.[19] Understanding the mechanisms that regulate the MDSC phenotype in the context of infection is important since this may represent a viable therapeutic target to improve disease outcomes.[4,20]

In the current study, we employed cellular indexing of transcriptomes and epitopes by sequencing (CITE-seq), which revealed that although F4/80$^+$MHCII$^+$ MDSCs share marker expression with G-MDSCs (Ly6G$^+$Ly6C$^+$CD11b^{high}), they represent a transcriptionally distinct population during PJI with increased cytokine (TNF and IL-6) production and transcriptional pathways associated with cytokine activation, inflammatory cell death, and cellular differentiation. We leveraged an adoptive transfer approach of G-MDSCs from CD45.1 mice into CD45.2 recipients to track their plasticity during S. *aureus* PJI, which demonstrated that G-MDSCs acquire a monocyte-like phenotype through the acquisition of F4/80 and MHCII expression and exhibit potent T-cell suppressive activity. These results highlight the plasticity in MDSC phenotypes during biofilm infection that may influence the chronicity of PJI.

2. Materials and methods

2.1 Mice

C57BL/6J (RRID:IMSR_JAX:000644), IL-10 KO (RRID:IMSR_JAX:002251), and congenic B6.SJL CD45.1 (RRID:IMSR_JAX:002014) mice were purchased from The Jackson Laboratory and maintained in-house at the University of Nebraska Medical Center (UNMC). Equal numbers of male and female mice at 8 to 10 wk of age were used for all experiments. This study was conducted in accordance with the recommendations in the Guide for the Care and Use of Laboratory Animals of the National Institutes of Health. The protocol was approved by the UNMC Institutional Animal Care and Use Committee (18-013-03).

2.2 Mouse model of S. *aureus* PJI

The S. *aureus* LAC 13C strain used in this study was derived from a USA300 clinical isolate recovered from a skin and soft tissue infection.[21,22] Prior to each experiment, bacteria were freshly streaked onto trypticase soy agar enriched with 5% sheep blood. A single colony was then inoculated into brain–heart infusion broth and grown overnight in a baffled flask (10:1 flask/volume ratio, 37 °C, 250 rpm). The overnight culture was washed twice with phosphate-buffered saline (PBS) and diluted to 5×10^5 colony-forming units (CFU)/mL to establish PJI in mice as previously described.[9–11,23,24] Briefly, C57BL/6J wild-type (WT) or IL-10 KO mice were anesthetized with an intraperitoneal injection of ketamine/xylazine, and a parapatellar arthrotomy was performed. A hole was created in the femoral intercondylar notch using a 26-gauge needle to insert an orthopedic-grade K-wire (0.6 mm diameter, nickel titanium; Custom Wire Technologies) that was inoculated with 2 µL (10^3 CFU) of S. *aureus* in PBS at the tip of the implant. The inner and outer incisions were closed using 6-0 polyglycolic acid and nylon suture, respectively. Buprenex slow release (Buprenex SR) was administered for pain relief, and mice were closely monitored following surgery, whereupon they exhibited normal ambulatory behavior.

2.3 Quantification of leukocyte infiltrates

At the indicated day postinfection, mice were euthanized using an overdose of inhaled isoflurane. Next, implant-associated tissue was excised and homogenized using the blunt end of a syringe and passed through a 70-µm filter to obtain a single-cell suspension, and red blood cells were lysed. For flow cytometry, Fc receptors were blocked using TruStain FcX (RRID: AB_1574973), and samples were stained with a panel of antibodies including CD45-PE-Cy7 (RRID:AB_312979) or -APC (RRID: AB_312977), Ly6C-APC-Cy7 (RRID:AB_1727555) or -PerCP-Cy5.5 (RRID:AB_1727558), Ly6G–Pacific Blue (RRID:AB_2251161) or -PE (RRID: AB_1186099), F4/80–Brilliant Violet 510 (RRID:AB_2562622) or -PE-Cy7 (RRID: AB_893490), CD11b–Alexa Fluor 700 (RRID:AB_493705) or -FITC (RRID: AB_312789), and MHCII (I-A/I-E)–Brilliant Violet 605 (RRID: AB_2565894) in combination with a fixable UV live/dead stain (BioLegend or Invitrogen). For adoptive transfer experiments, CD45.1-PE-Dazzle 594 (RRID:AB_2564295) and CD45.2-APC (RRID: AB_389211) were used to identify adoptively transferred vs endogenous leukocytes, respectively. Samples were processed using a LSR Fortessa ×50 and analyzed using FlowJo (RRID:SCR_008520).

2.4 T-cell suppression assay

CD4$^+$ T cells were collected from the spleen of a naive mouse and purified using a CD4$^+$ T-cell isolation kit (Miltenyi) following the manufacturer's instructions. T cells were stained using Cell Proliferation Dye eFluor 670 (eBioscience; 2.5 µM), then washed and resuspended in complete medium containing mouse recombinant IL-2 (100 ng/mL). T-cell proliferation was induced using CD3/CD28 Dynabeads. To determine the ability of leukocyte populations recovered from S. *aureus* PJI to inhibit T-cell proliferation, G-MDSCs, PMNs, F480$^+$MHCII$^+$ MDSCs, and monocytes were sorted from the implant-associated tissue of mice at day 14 post-infection with a BD Biosciences FACSAria or FACSAria II using the antibody panel described above. Sorted leukocyte populations were cocultured with T cells at a 1:1 ratio and incubated at 37 °C for 3 d, whereupon cells were analyzed on a BD Biosciences LSRII Y/G. T-cell proliferation was determined by the progressive loss of the cell proliferation dye.

2.5 Morphological analysis

To compare the morphology of F4/80$^+$MHCII$^+$ MDSCs to other leukocyte infiltrates during PJI, cytospin slides were prepared for each fluorescence-activated cell sorting (FACS)-purified population. Slides were stained with Wright–Giemsa and provided in a blinded fashion to a board-certified hematopathologist, who performed differential counts. Slides were also imaged using a Leica AperioCS2 scanning system to report cellular morphology.

2.6 CITE-seq and bioinformatics

2.6.1 Cell recovery and barcoding

Implant-associated tissue was collected from WT mice at day 14 following S. *aureus* PJI and homogenized, and after red blood cells lysis, Fc receptors were blocked as described above. Samples were

stained with CD45-APC (RRID: AB_312977), Ly6G-PE (RRID: AB_1186099), Ly6C-PerCP-Cy5.5 (RRID:AB_1727558), and Live/Dead fixable blue stain, whereupon live Ly6G$^+$Ly6C$^+$ and Ly6C$^+$Ly6G$^-$ cells were collected using a BD Biosciences FACSAria. Next, these populations were labeled using TotalSeq-B0114 F4/80 (RRID: AB_2819847) and TotalSeq-B0117 I-A/I-E (RRID: AB_2832367) barcoded antibodies (BioLegend) following the manufacturer's protocol. The postsort viability of Ly6C$^+$Ly6G$^-$ and Ly6G$^+$Ly6C$^+$ populations was 79.6% and 89.4%, respectively, with minimal debris as determined using a Luna automated fluorescent cell counter (Logos Biosystems).

2.6.2 Library preparation and sequencing

Ly6G$^+$Ly6C$^+$ and Ly6C$^+$G$^-$ cells (13,627 and 1,624, respectively) were processed using a 10× Genomics platform by the UNMC Genomics Core. Briefly, single cells were lysed, and RNA was reverse-transcribed and barcoded using a Chromium Single-Cell 3′ Reagent Kit v3 (10× Genomics) according to the manufacturer's protocol. Illumina-compatible cDNA libraries were created and quantified by quantitative PCR using the KAPA Library Quant Kit (Illumina) and loaded at a concentration of 1.3 pM on an Illumina NovaSeq instrument. Samples were sequenced following the parameters suggested by 10× Genomics to an average read depth of 100,000 reads/cell. Alignment was completed using 10× Genomics Cell Ranger with the *Mus musculus* mm10 genome as a reference. The complete CITE-seq data set has been deposited in the Gene Expression Omnibus database (accession number GSE248640).

2.7 CITE-seq analysis

2.7.1 Quality assurance/quality control and normalization

Single-cell expression data were largely analyzed using Partek Genomics Suite (RRID:SCR_011860). Single-cell count output from Cell Ranger was imported into Partek Flow and split by feature type (antibody capture and gene expression), and quality control was performed independently on each feature to filter low-quality cells. For the antibody capture, a maximum count threshold of 5,000 was used to exclude protein aggregates, but no minimum was used since not every cell was expected to express either F4/80 or MHCII. Gene expression was also filtered based on counts (1,500 to 35,000), detected features (400 to 6,000), and percent mitochondrial counts (0% to 20%) to exclude potential doublets and nonviable cells. Each feature was then normalized independently. Antibody capture counts were normalized using a centered log-ratio as suggested for CITE-seq data.[25,26] Gene expression was normalized using counts per million, add 1, and log base e to allow for integration with the antibody capture data. The different feature counts were then merged for downstream analysis. Following this step, 12,998 (95.4%) and 1,220 (75.1%) of captured Ly6G$^+$Ly6C$^+$ and Ly6C$^+$Ly6G$^-$ cells, respectively, passed each feature's quality assurance/quality control and were included for gene/pathway analysis.

2.7.2 Exploratory analysis

The top 20 principal components were used for clustering, and differential expression analysis between each cluster was performed by computing biomarkers. Cell-type identities were annotated using SingleR[27] with the Immunological Genome Project (ImmGen; https://www.immgen.org/) as the reference data set. Cells that were identified as PMNs were selected and reclustered to assess granulocyte heterogeneity. To identify Ly6G$^+$Ly6C$^+$F480$^+$MHCII$^+$ cells within the data set, cells in the Ly6G$^+$Ly6C$^+$ sample were classified based on F4/80 and MHCII protein expression using the unique antibody barcodes. Cells with F4/80 signals >0.8 and MHCII >0.9 were classified as F480$^+$MHCII$^+$, whereas F4/80 <0.8 and MHCII <0.9 represented F4/80$^-$MHCII$^-$. These cutoffs were determined by F4/80 and MHCII expression on monocytes and macrophages in the Ly6C$^+$Ly6G$^-$ sample. A Hurdle model was used to determine differential gene expression and pathways enriched in the F480$^+$MHCII$^+$ population.

2.7.3 Intracellular cytokine staining

To assess TNF and IL-6 expression in leukocyte populations during PJI, intracellular staining was performed. Briefly, infected tissues were homogenized as described above; however, after red blood cell lysis, samples were resuspended in complete medium (RPMI + 10% fetal bovime serum [FBS] + 2 mM L-glutamine, 10 mM HEPES, antibiotic/antimycotic solution, and 50 µM β-mercaptoethanol) containing brefeldin A for 4 h. After Fc block, cells were stained with the same surface marker panel described above, treated with Cyto-Fast fix/perm buffer, and incubated with TNF-PerCP-Cy5.5 (RRID:AB_961434) or IL-6-APC (RRID: AB_10694868) in Cyto-Fast Perm wash solution (all from BioLegend). Samples were processed using either a BD Biosciences LSRII Y/G or LSR Fortessa ×50 and analyzed using FlowJo to report TNF and IL-6 expression in G-MDSCs (Ly6G$^+$Ly6C$^+$CD11b^{high}F4/80$^-$), PMNs (Ly6G$^+$CD11b^{low}F4/80$^-$), F4/80$^+$MHCII$^+$ MDSCs (Ly6G$^+$Ly6C$^+$CD11b^{high}F4/80$^+$MHCII$^+$), monocytes (Ly6C$^+$Ly6G$^-$F4/80$^-$), and macrophages (Ly6C$^{+/-}$Ly6G$^-$F4/80$^+$MHCII$^+$).

2.7.4 Adoptive transfer

Primary G-MDSCs were prepared in vitro from the bone marrow of CD45.1 congenic mice as previously described.[11] Briefly, CD45.1-G-MDSCs were propagated for 4 d in RPMI-1640 supplemented with 10% FBS, 2 mM L-glutamine, 10 mM HEPES, antibiotic/antimycotic solution, 50 µM β-mercaptoethanol, 40 ng/mL granulocyte-macrophage colony-stimulating factor, and 40 ng/mL granulocyte colony-stimulating factor with 40 ng/mL IL-6 added on day 3 of culture. At day 4, G-MDSCs were enriched using anti-Ly6G microbeads (Miltenyi Biotec) and further purified by FACS to isolate live CD45.1$^+$ G-MDSCs that were F4/80 and MHCII negative (Ly6G$^+$Ly6C$^+$CD11b^{high}F4/80$^-$MHCII$^-$) using the antibody panel above. Purified CD45.1-G-MDSCs (7.5×10^5 per mouse) were injected into the knee of IL-10 KO mice (CD45.2) at day 14 following *S. aureus* PJI, whereupon the phenotype of CD45.1-G-MDSCs was determined 24 h later. To confirm that adoptively transferred G-MDSCs were retained at the site of injection, cells were labeled with Qtracker 655 (Invitrogen) prior to transfer and then imaged 24 h later using an *In Vivo* Imaging System (IVIS; PerkinElmer).

2.7.5 Statistics and figure generation

For CITE-seq data analysis, significant differentially expressed genes or enriched pathways were determined using a false discovery rate-adjusted *P* value of <0.05. Significant differences between groups for flow cytometry were determined using a 1-way analysis of variance with Tukey's multiple comparisons test in GraphPad Prism (GraphPad Software), where a *P* value of <0.05 was considered statistically significant.

3. Results

3.1 F4/80$^+$MHCII$^+$ MDSCs represent a minor but highly suppressive population during *S. aureus* PJI

MDSCs are a heterogenous, immature myeloid population that accumulates during pathologies such as cancer or chronic infection.[1,4] *S. aureus* PJI is defined by a dominant G-MDSC infiltrate based on cell morphology, surface marker expression, and gene expression.[9–11,28] However, after incorporating additional myeloid markers in our flow panel, a small population of Ly6G$^+$Ly6C$^+$CD11b^{high} G-MDSCs (3% to 5%) were also found to coexpress F4/80 and MHCII (Fig. 1). Since these markers are typically associated with monocytes/macrophages,[29] Ly6G$^+$Ly6C$^+$CD11b^{high}F4/80$^+$MHCII$^+$ cells were purified by FACS at day 14 postinfection, whereupon cell morphology was evaluated using cytospins. Ly6G$^+$Ly6C$^+$CD11b^{high}F4/80$^+$MHCII$^+$ cells were a heterogenous population of immature granulocytes and monocytes as revealed by banded and large, round nuclei (Supplementary Fig. 1), similar to that previously reported for G-MDSCs.[9]

We next examined the functional properties of F4/80$^+$MHCII$^+$ MDSCs by evaluating their ability to suppress T-cell proliferation, a hallmark of MDSC activity. F4/80$^+$MHCII$^+$ MDSCs, G-MDSCs, PMNs, and monocytes were purified at day 14 following *S. aureus* PJI by FACS and cocultured with CD4$^+$ T cells at a 1:1 ratio. F4/80$^+$MHCII$^+$ MDSCs significantly inhibited T-cell proliferation, similar to well-characterized G-MDSCs, whereas monocytes and PMNs had minimal suppressive activity (Fig. 2). Collectively, these results suggest that F4/80$^+$MHCII$^+$ MDSCs may represent a previously unidentified population of MDSCs in the context of *S. aureus* biofilm that possess T-cell inhibitory capacity.

3.2 F4/80$^+$MHCII$^+$ MDSCs are a transcriptionally distinct cluster that arises during *S. aureus* PJI

We next investigated the transcriptional profile of F4/80$^+$MHCII$^+$ MDSCs during *S. aureus* PJI using CITE-seq.[25] This technology utilizes single-cell sequencing coupled with barcoded antibodies against surface markers to assist with cellular identification. This is important since RNA expression of leukocyte surface markers does not always reflect protein abundance,[30] which was observed in our study since *adgre1* and *h2-ab1* gene expression was not highly correlated with F4/80 and MHCII protein abundance, respectively (Supplementary Fig. 2).

CITE-seq was performed on FACS-purified G-MDSC (Ly6G$^+$Ly6C$^+$CD11b^{high}) and monocyte/macrophage (Ly6C$^+$Ly6G$^-$CD11b^{high}) infiltrates at day 14 following *S. aureus* PJI. Monocytes/macrophages were used to compare transcriptional similarity with F4/80$^+$MHCII$^+$ MDSCs that exhibited monocyte-

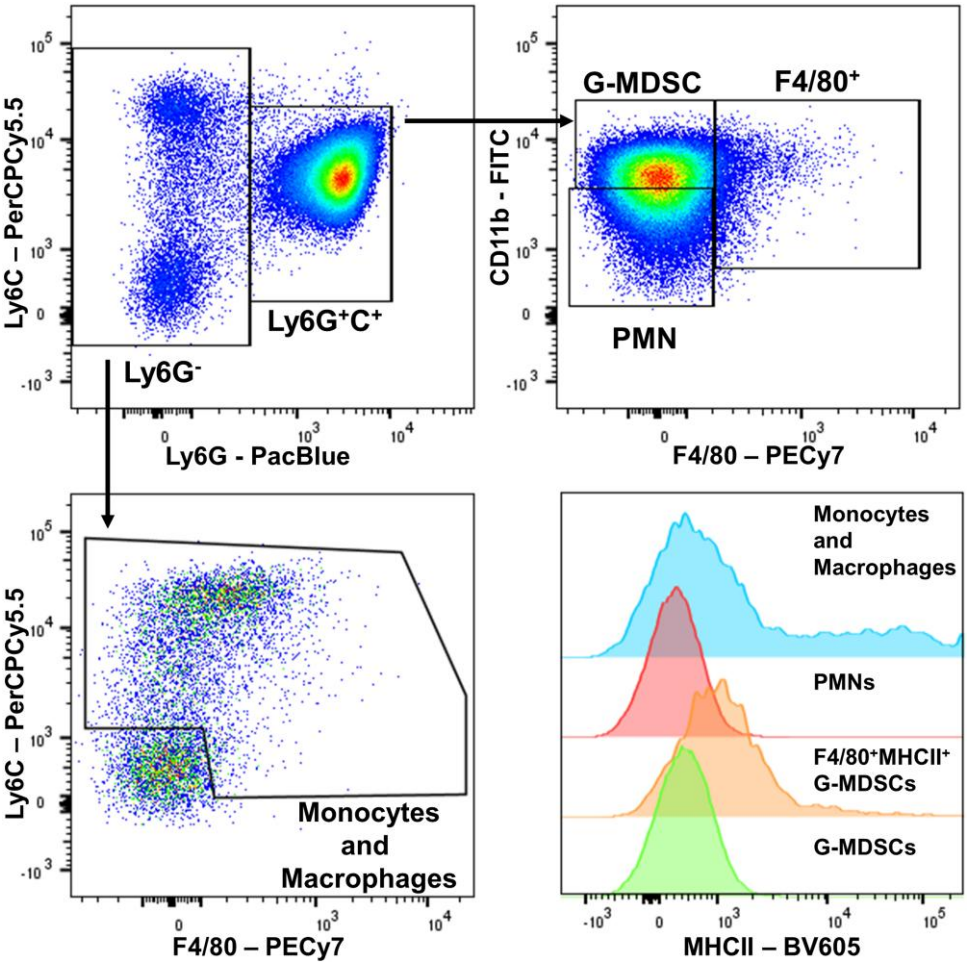

Fig. 1. A subpopulation of G-MDSCs expresses F4/80 and MHCII during *S. aureus* biofilm infection. Leukocytes from the implant-associated tissue of C57BL/6J mice at day 14 following *S. aureus* PJI were analyzed using flow cytometry. Live singlets expressing CD45 were gated to identify G-MDSCs (Ly6G$^+$Ly6C$^+$CD11b^{high}F4/80$^-$), neutrophils (Ly6G$^+$CD11b^{low}F4/80$^-$), monocytes and macrophages (Ly6C$^+$Ly6G$^-$), and F4/80$^+$ MDSCs (Ly6G$^+$Ly6C$^+$F4/80$^+$). MHC class II expression in each population is shown in the histogram. Dot plots and histograms are concatenated from 5 mice and are representative of 3 independent experiments.

like properties. Ly6G$^+$Ly6C$^+$ cells were examined for F4/80 and MHCII surface protein abundance, where 2,724 cells (21.0%) were identified as F4/80$^+$MHCII$^+$, whereas 8,136 cells (62.6%) were F4/80$^-$MHCII$^-$. The remaining cells were single-positive for either F4/80 or MHCII (16.4%) (Supplementary Fig. 3).

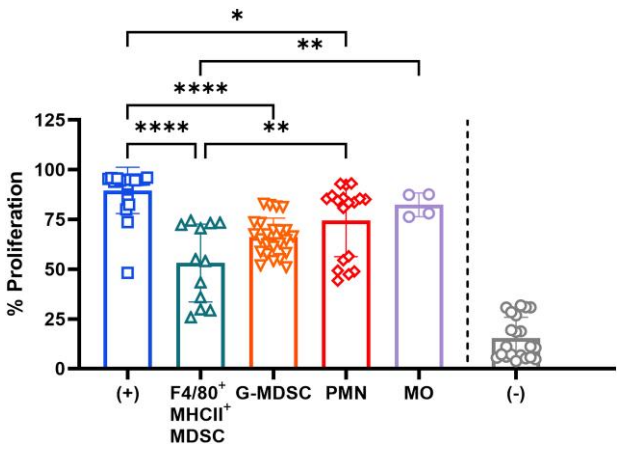

Fig. 2. F4/80$^+$MHCII$^+$ MDSCs suppress T-cell proliferation. F4/80$^+$MHCII$^+$ MDSCs, G-MDSCs, neutrophils (PMNs), and monocytes (MOs) were purified from implant-associated tissue of C57BL/6J mice at day 14 following *S. aureus* PJI by FACS. Leukocytes were cocultured at a 1:1 ratio with CD4$^+$ T cells isolated from the spleen of a naive mouse for 72 h in the presence of CD3/CD28 Dynabeads to induce polyclonal T-cell activation. Proliferation was assessed by flow cytometry where the positive control (+) reflects T cells with CD3/CD28 stimulation and negative control (–) represents T cells only ($n = 4$ to 24 from 5 independent experiments; $^*P < 0.05$, $^{**}P < 0.01$, $^{****}P < 0.0001$; 1-way analysis of variance with Tukey's multiple comparisons test). The number of monocytes recovered from infected tissues was limiting, which reflects the lower n for this group.

All cells were subjected to dimensionality reduction and clustering to identify groups of transcriptionally related cells. Ly6G$^+$Ly6C$^+$ MDSCs and Ly6C$^+$Ly6G$^-$ monocytes separated into distinct clusters with minimal overlap (Fig. 3A), supporting the stringency of the methodology. Nine total clusters were observed (Fig. 3B), with clusters 1 to 5 identified as PMNs, whereas clusters 6 to 8 consisted mainly of monocytes and macrophages (Fig. 3C), as determined by automated cell-type identification using SingleR.[27] Ly6G$^+$Ly6C$^+$F4/80$^+$MHCII$^+$ cells were mainly represented in cluster 4, accounting for 63.2% of cells in this group (Fig. 3D), suggesting they are a transcriptionally distinct population. The SingleR package is not capable of discriminating between G-MDSCs and PMNs and classifies both cell types as granulocytes. However, using published gene sets to bioinformatically define each population,[31,32] cluster 5 displayed higher expression of genes suggestive of PMNs (i.e. *cd177*), whereas clusters 1 to 3 expressed genes associated with G-MDSCs (i.e. *cd84*, *arg2*, *wfdc17*, and *clec4d*) (Fig. 4). Interestingly, cluster 4 (mainly comprising F4/80$^+$MHCII$^+$ MDSCs) also had increased expression of G-MDSC genes similar to clusters 1 to 3 (Fig. 4). These observations suggest that F4/80$^+$MHCII$^+$ MDSCs may represent an altered G-MDSC phenotype with a distinct transcriptome.

3.3 F4/80$^+$MHCII$^+$ MDSCs are typified by increased cytokine production

To further understand transcriptional distinctions between PMNs, G-MDSCs, and F4/80$^+$MHCII$^+$ MDSCs, all granulocytes from our CITE-seq analysis were selected for dimensionality

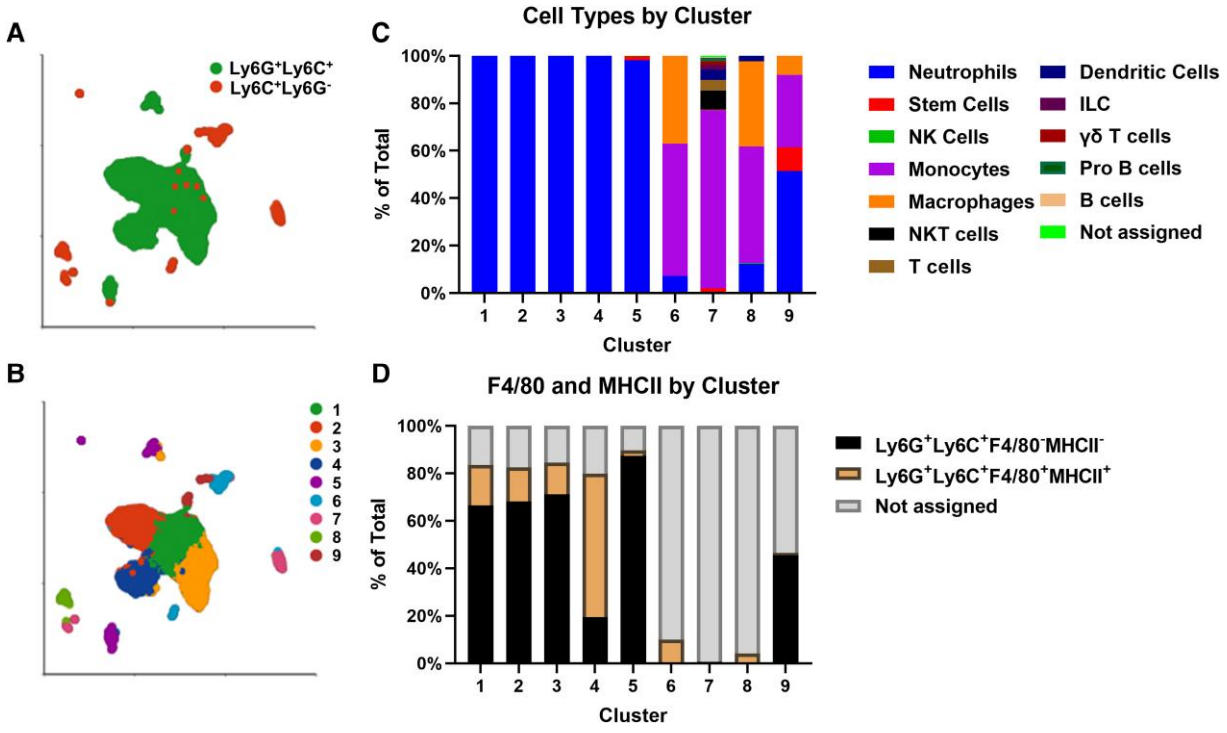

Fig. 3. F4/80$^+$MHCII$^+$ MDSCs express a unique transcriptional signature. CITE-seq was performed on FACS-purified Ly6G$^+$Ly6C$^+$ cells and monocytes (Ly6C$^+$Ly6G$^-$) collected at day 14 following *S. aureus* PJI and labeled with F4/80 and MHCII barcoded antibodies. (A) Uniform manifold approximation and projection (UMAP) depicting the separation of the Ly6G$^+$Ly6C$^+$ G-MDSC population and Ly6C$^+$Ly6G$^-$ monocytes and (B) UMAP with graph-based clustering of both samples. (C) The proportion of cell types within each graph-based cluster as identified by an automated cell-type identification program (SingleR) using Immgen as a reference database and (D) the proportion of F4/80$^+$MHCII$^+$ and F4/80$^-$MHCII$^-$ cells within the Ly6G$^+$Ly6C$^+$ population ("not assigned" reflects cells from the Ly6G$^+$Ly6C$^+$ sample that were F4/80 or MHCII single positive or from the monocyte sample; see Supplementary Fig. 4 for additional information).

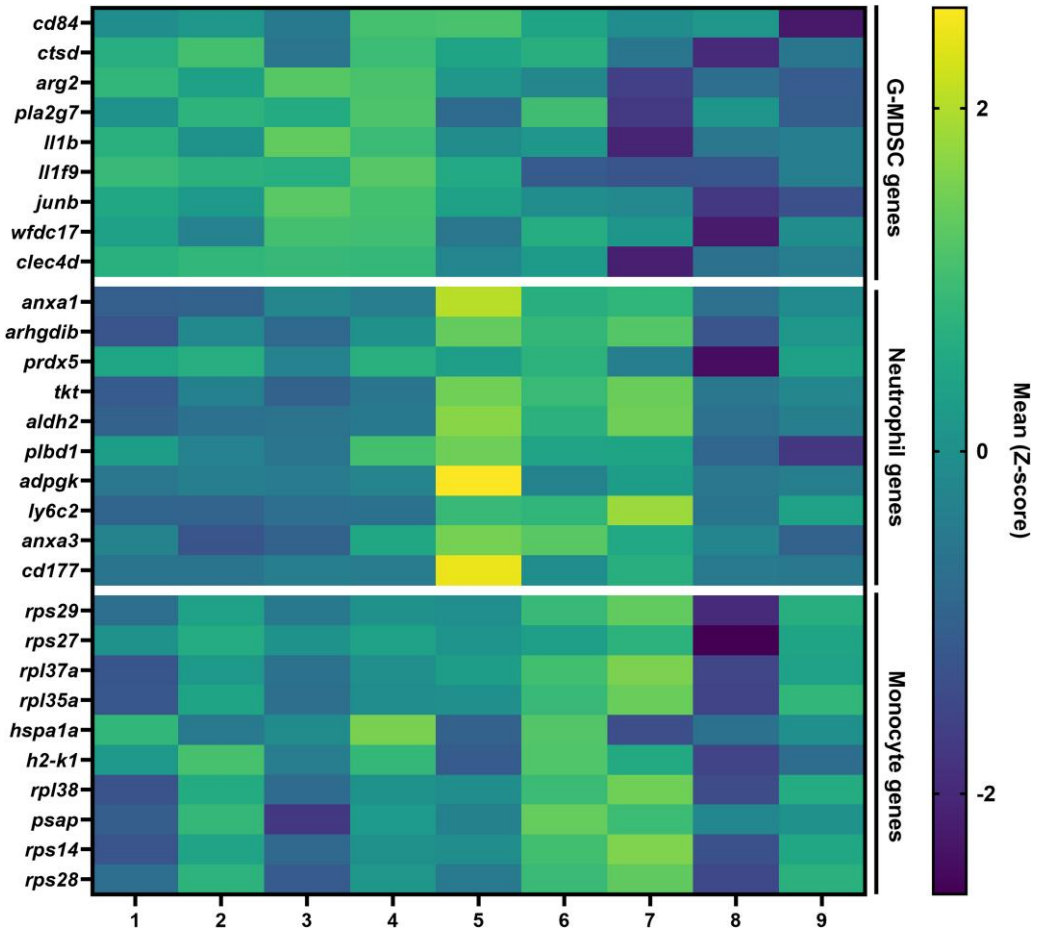

Fig. 4. F4/80$^+$MHCII$^+$ MDSCs express MDSC-like genes. A heatmap depicts the mean (z-score) of a gene list containing MDSC, neutrophil, and monocyte genes for each graph-based cluster identified.

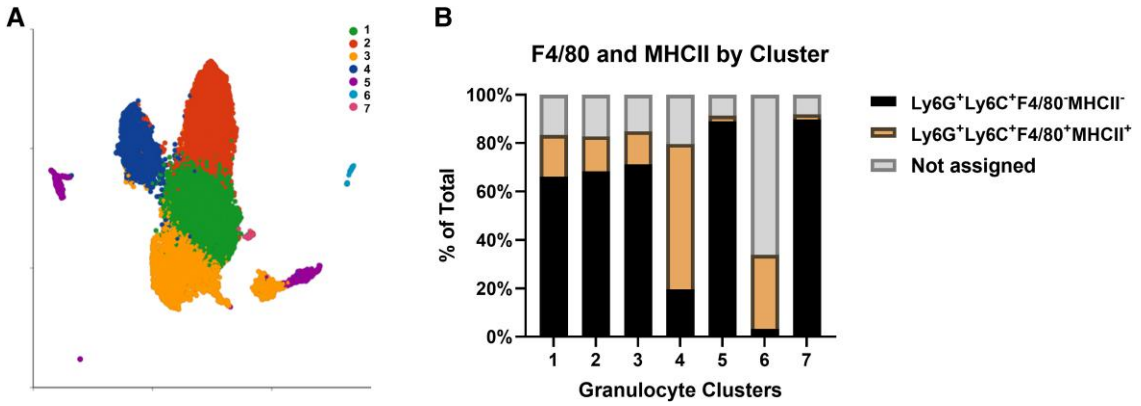

Fig. 5. A distinct transcriptional profile of F4/80$^+$MHCII$^+$ MDSCs is evident within heterogeneous granulocyte clusters. Granulocytes were selected from the CITE-seq data and underwent a new round of dimensionality reduction and graph-based clustering, which (A) resulted in a UMAP plot with 7 distinct clusters. (B) The proportion of F4/80$^+$ and MHCII$^+$ cells within each graph-based cluster is shown.

reduction and clustering. Again, F4/80$^+$MHCII$^+$ MDSCs were found mainly in cluster 4, comprising 60% of the cells in this population (Fig. 5). Genes that were significantly differentially expressed in cluster 4 included a hypoxanthine transporter (*slc23a3*), peptide cross-linking/cysteine-type endopeptidase inhibitor activity (*ctsdc5* and *stfa2*), cell–cell adhesion (*mpzl2* and *thbs4*), and serum amyloid A1 (*saa1*) (Fig. 6 and Table 1). We next performed differential expression analysis comparing F4/80$^+$MHCII$^+$ MDSCs vs F4/80$^-$MHCII$^-$ granulocytes to more specifically examine pathways enriched in the former. Many pathways were significantly increased in F4/80$^+$MHCII$^+$ MDSCs that were indicative of an activated, inflammatory state (response to stimulus/molecule of bacterial origin [GO:0050896/GO:0002237], positive regulation of metabolic process [GO:0009893], positive regulation of cytokine production [GO:0001819], response to cytokine [GO:0034097]), positive regulation of programmed cell death [GO:0043067 and

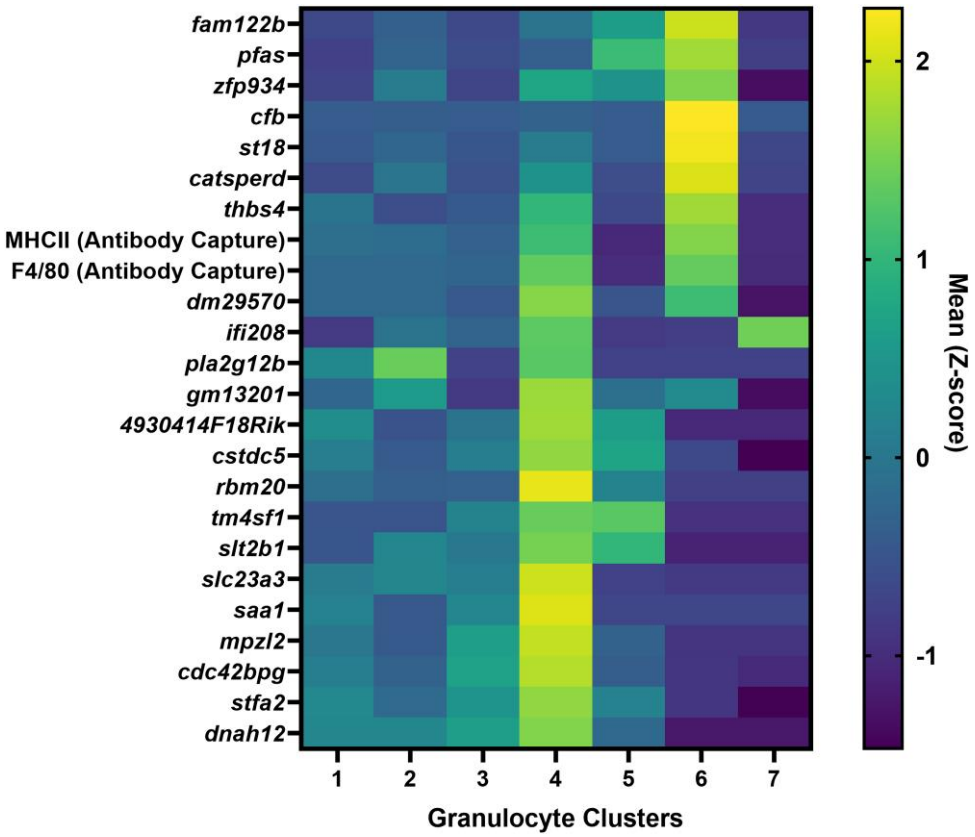

Fig. 6. F4/80⁺MHCII⁺ MDSCs express a distinct transcriptional profile compared to other granulocyte populations. Differential expression was performed to identify genes that were differently regulated in F4/80⁺MHCII⁺ MDSCs vs the other granulocyte subsets. The top 22 features are shown as means for each cluster (z-scores). Signals for MHCII and F4/80 antibody reactivity are also shown.

Table 1. Differentially expressed genes in cluster 4 (F4/80⁺MHCII⁺ MDSCs) compared to other granulocyte clusters.

Cluster 4	P value	Fold-change
cdc42bpg	<0.001	1.619
ifi208	<0.001	1.519
slc23a3	<0.001	1.518
cstdc5	<0.001	1.502
stfa2	<0.001	1.647
catsperd	<0.001	1.520
mpzl2	<0.001	1.678
gm13201	<0.001	1.565
sult2b1	<0.001	1.595
gm29570	<0.001	1.981
thbs4	<0.001	1.661
st18	<0.001	1.654
rbm20	<0.001	1.594
zfp934	<0.001	1.609
cfb	0.001	1.595
fam122b	0.001	1.580
tm4sf1	0.005	1.501
saa1	0.006	3.454
4930414F18Rik	0.012	1.638

GO:0043068] and positive regulation of IL-1 β production [GO:0032731]) (Table 2). Several genes were significantly increased in F4/80⁺MHCII⁺ MDSCs vs F4/80⁻MHCII⁻ cells, including *Tnf* (3.45-fold) (Figs. 7 and 8A). To confirm these bioinformatic findings, intracellular cytokine staining was performed on leukocytes recovered from *S. aureus* PJI, where Ly6G⁺Ly6C⁺F4/80⁺MHCII⁺ MDSCs produced the highest amount of TNF compared to other leukocyte populations (Fig. 8B and 8C). IL-6 expression was also significantly higher in F4/80⁺MHCII⁺ MDSCs (Supplementary

Table 2. Enriched pathways within cluster 4 (F4/80⁺MHCII⁺ MDSCs) compared to other granulocyte clusters.

Gene set	Description	Enrichment score	P value
GO:0050896	Response to stimulus	62.470	<0.001
GO:0009893	Positive regulation of metabolic process	52.764	<0.001
GO:0043067	Regulation of programmed cell death	49.357	<0.001
GO:0002237	Response to molecule of bacterial origin	40.329	<0.001
GO:0001819	Positive regulation of cytokine production	40.171	<0.001
GO:0034097	Response to cytokine	39.875	<0.001
GO:0043068	Positive regulation of programmed cell death	38.626	<0.001
GO:0007166	Cell surface receptor signaling pathway	33.799	<0.001
GO:0010647	Positive regulation of cell communication	30.545	<0.001
GO:0001666	Response to hypoxia	29.139	<0.001
GO:0032731	Positive regulation of IL-1 β production	26.985	<0.001
GO:0030154	Cell differentiation	23.338	<0.001
GO:1903131	Mononuclear cell differentiation	13.410	<0.001

Gene set enrichment was performed on the genes identified in graph-based cluster 4 compared to other granulocytes to determine significantly enriched pathways within this cluster ($P < 0.05$). Select pathways are shown.

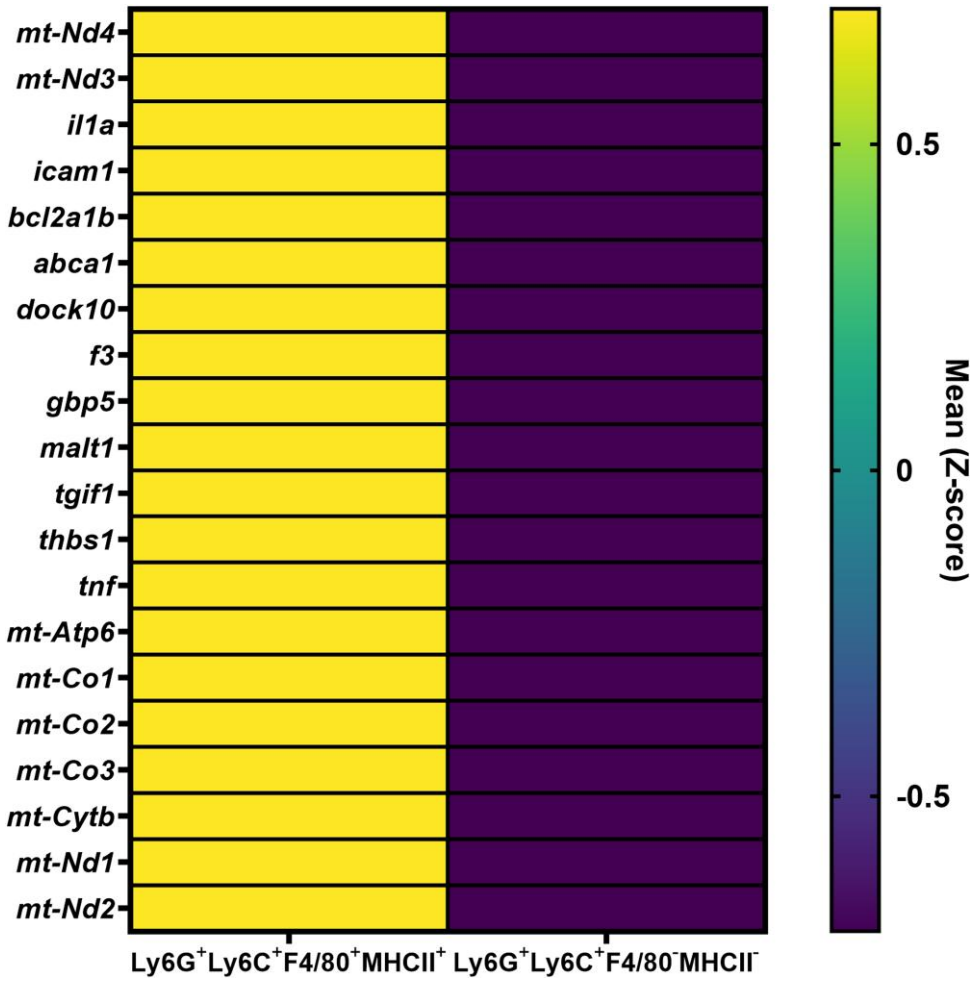

Fig. 7. Differentially expressed genes between F4/80$^+$MHCII$^+$ MDSCs and F4/80$^-$MHCII$^-$ granulocytes. A hurdle model was used to identify significantly differentially expressed genes between F4/80$^+$MHCII$^+$ MDSCs and F4/80$^-$MHCII$^-$ granulocytes within the Ly6G$^+$Ly6C$^+$ sample. The top 20 differentially enriched genes (by fold-change, $P < 0.05$) are shown using a heatmap depicting the mean for each population (z-score).

Fig. 4), again supporting their unique features compared to other leukocyte subsets infiltrating the infected tissue. Mitochondrial genes were also among the top differentially expressed genes in F4/80$^+$MHCII$^+$ MDSCs (Fig. 7 and Supplementary Fig. 5).

3.4 The microenvironment during *S. aureus* PJI drives G-MDSCs to acquire a monocyte-like phenotype

Since pathways related to cell differentiation (GO:0030154) and mononuclear cell differentiation (GO:1903131) were significantly upregulated in F4/80$^+$MHCII$^+$ MDSCs (Table 2), this suggested a possible transition of F4/80$^+$MHCII$^+$ cells from a granulocytic (G-MDSC) to a monocyte phenotype. To explore this possibility from a biological perspective, we utilized an adoptive transfer approach with G-MDSCs expanded from the bone marrow of CD45.1$^+$ B6.SJL congenic mice, whereas C57BL/6J recipients express CD45.2.[33] The congenic CD45 allele does not affect function related to granulocyte activity[34] and permits the discrimination of donor G-MDSCs from endogenous leukocytes using CD45.1- and CD45.2-specific antibodies. We have previously shown that G-MDSCs expanded from the mouse bone marrow express the same cell surface markers as their in vivo counterparts (Ly6G$^+$Ly6C$^+$CD11b^{high}) and suppress T-cell proliferation;[35] therefore, these cells represent a suitable surrogate to investigate the fate of G-MDSCs in vivo. We were unable to leverage Cre-Lox fate mapping approaches[36] since a unique Cre-driver for G-MDSCs has not yet been identified based on their similarity to PMNs.

To determine whether G-MDSCs exhibit plasticity during *S. aureus* PJI, FACS-purified Ly6G$^+$Ly6C$^+$CD11b^{high}F4/80$^-$MHCII$^-$ G-MDSCs derived from naive CD45.1$^+$ B6.SJL mice were injected subcutaneously into the soft tissue surrounding the knee joint of IL-10 KO animals (CD45.2) at day 14 postinfection (Fig. 9A). This time point and the use of IL-10 KO mice were selected based on pilot studies where the greatest survival of adoptively transferred G-MDSCs was observed. To ensure that G-MDSCs were retained at the site of infection, CD45.1$^+$ G-MDSCs were labeled with Quantum dots, where fluorescent signals were localized to the implant-associated tissue (Supplementary Fig. 6). Mice were sacrificed at 24 h following G-MDSC transfer to define their phenotype. Only ~200 CD45.1$^+$ cells were recovered per animal, representing approximately 0.03% of the transferred population. This revealed a high attrition rate of G-MDSCs during infection, likely due to the production of cytotoxic molecules by *S. aureus* biofilm.[37,38] Nevertheless, CD45.1$^+$ G-MDSCs that survived adoptive transfer acquired MHCII and F4/80 expression concomitant with decreased Ly6G, Ly6C, and CD11b levels compared to endogenous G-MDSCs (CD45.2$^+$), suggesting the acquisition of a more monocyte-like phenotype (Fig. 9B). Taken together, these results

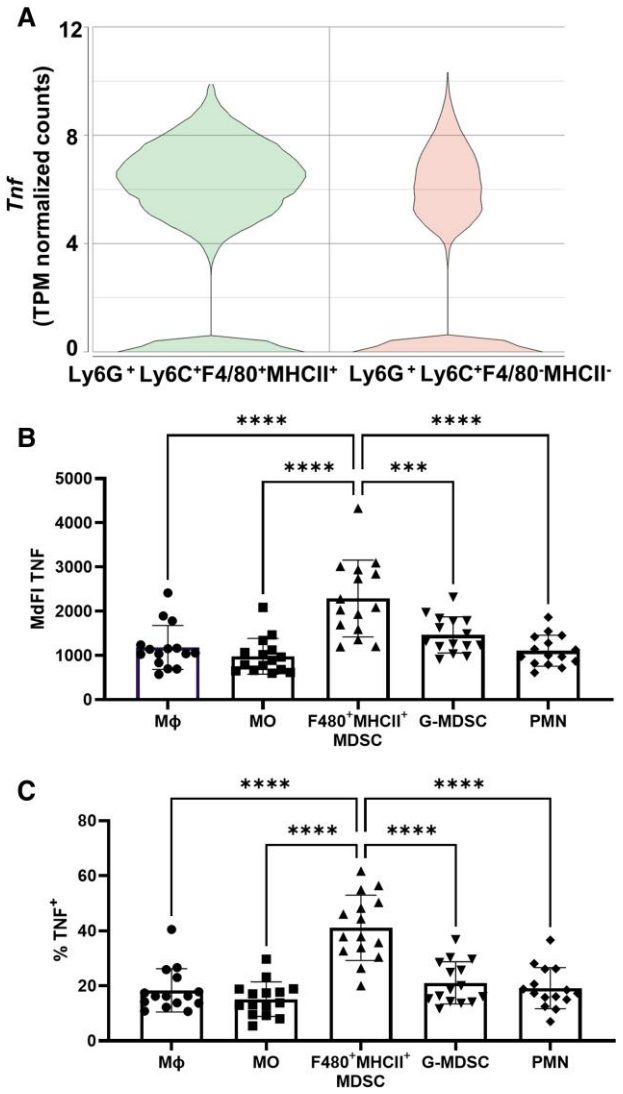

Fig. 8. F4/80$^+$MHCII$^+$ MDSCs produce high amounts of TNF in vivo. (A) Violin plot depicting *Tnf* transcript expression in F4/80$^+$MHCII$^+$ MDSCs and F4/80$^-$MHCII$^-$ granulocytes expressed as transcripts per million (TPM) normalized counts. Intracellular staining for TNF was performed on leukocytes recovered from implant-associated tissue at day 14 following *S. aureus* PJI depicted as (B) median fluorescence intensity (MdFI) or (C) percent positive cells ($n = 15$ mice/biological replicates; $^{***}P < 0.001$, $^{****}P < 0.0001$; 1-way analysis of variance with Tukey's multiple comparisons test).

support the plasticity of a G-MDSC subpopulation during *S. aureus* PJI that acquires F4/80 and MHCII expression, while remaining highly immunosuppressive together with increased TNF and IL-6 production.

4. Discussion

This work has established that a subpopulation of G-MDSCs acquires F4/80 and MHCII expression during biofilm infection. Prior work has shown that M-MDSCs can mature into tumor-associated macrophages and dendritic cells;[14,39] however, G-MDSCs are typically considered terminal cells with a short half-life.[13] Recently, it was reported that a large portion of the G-MDSC pool in tumor-bearing mice was derived from monocyte-like precursors and M-MDSCs,[18,40] setting a precedent for MDSC conversion between subtypes. Our data support G-MDSC plasticity, where cells can acquire a more monocyte-like phenotype during *S. aureus* PJI typified by increased F4/80 and MHCII expression. This is interesting, as both markers are typically associated with monocytes/macrophages, yet F4/80$^+$MHCII$^+$ MDSCs displayed potent T-cell suppressive activity. This is not unprecedented, as others have described a nonmonocytic, nongranulocytic MDSC population that expresses MHCII.[41] Future studies are needed to determine whether the acquisition of monocyte markers may occur in other pathologies where G-MDSCs are present and whether the mechanism of T-cell inhibition by F4/80$^+$MHCII$^+$ MDSCs is similar to or distinct from conventional G-MDSCs.

Since F4/80$^+$MHCII$^+$ MDSCs comprised a small proportion of leukocytes at the site of PJI, extensive ex vivo functional studies and bulk RNA sequencing were prohibitive. To circumvent these issues, we utilized CITE-seq to analyze the transcriptome of F4/80$^+$MHCII$^+$ MDSCs that leveraged the cell surface markers of this population. Interestingly, Ly6G$^+$Ly6C$^+$F4/80$^+$MHCII$^+$ MDSCs identified by CITE-seq comprised a larger proportion of the Ly6G$^+$Ly6C$^+$ population (21%) than was detected by flow cytometry (5%), reflecting differences in sensitivity between these techniques. We then used an unbiased automated cell-type identification program, SingleR,[27] which classified cells based on large Immgen reference data sets. Even though our G-MDSCs of interest expressed F4/80 and MHCII, which are expressed on monocytes/macrophages, these cells were identified as PMNs. It is not unexpected that G-MDSCs would be identified as PMNs in this reference data set, since the program is not capable of making these types of refined calls. Indeed, we have previously reported that G-MDSCs group with PMNs in other single-cell RNA sequencing experiments,[12,31] where separation into G-MDSCs vs PMNs was based on published gene sets.

While F4/80$^+$MHCII$^+$ MDSCs were classified as PMNs by the automated cell-type identification program, pathway analysis indicated that mononuclear cell differentiation was enriched in the former. This suggests a novel granulocytic-to-monocytic phenotypic conversion that has not previously been reported for G-MDSCs in the context of *S. aureus* infection. Furthermore, pathways involved in the response to cytokines and production of cytokines were enriched in F4/80$^+$MHCII$^+$ MDSCs, which we confirmed by intracellular cytokine staining for IL-6 and TNF. We focused on TNF because of its reported role in promoting MDSC activation[42,43] and the fact that TNFR expression is robust on monocytes/macrophages and the F480$^+$MHCII$^+$ MDSC population that we identified acquired the expression of monocyte markers. Since F4/80$^+$MHCII$^+$ MDSCs were highly immunosuppressive, it may seem contradictory that they would produce this proinflammatory cytokine; however, it has been shown that autocrine TNF secretion by MDSCs enhances their suppressive activity by upregulating *Nos2*.[42] Additionally, the "2-signal model" for MDSC expansion and activation suggests that MDSCs require proinflammatory activation signals at the site of inflammation to trigger their immunosuppressive properties,[1,44] which is supported by the finding that TNF influences MDSC accumulation and survival during cancer.[45] This raises the possibility that TNF production by F4/80$^+$MHCII$^+$ MDSCs may be important for activating newly recruited G-MDSCs at the site of PJI. However, this possibility would be challenging to assess since F4/80$^+$MHCII$^+$ MDSCs lack a unique surface marker, making targeted depletion difficult. In addition, our CITE-seq data set did not identify a unique or highly differentially expressed gene encoding a cell surface protein that could be used for this purpose. Like TNF, IL-6 expression was also significantly elevated in F4/80$^+$MHCII$^+$ MDSCs compared to the other leukocyte populations infiltrating the infected joint,

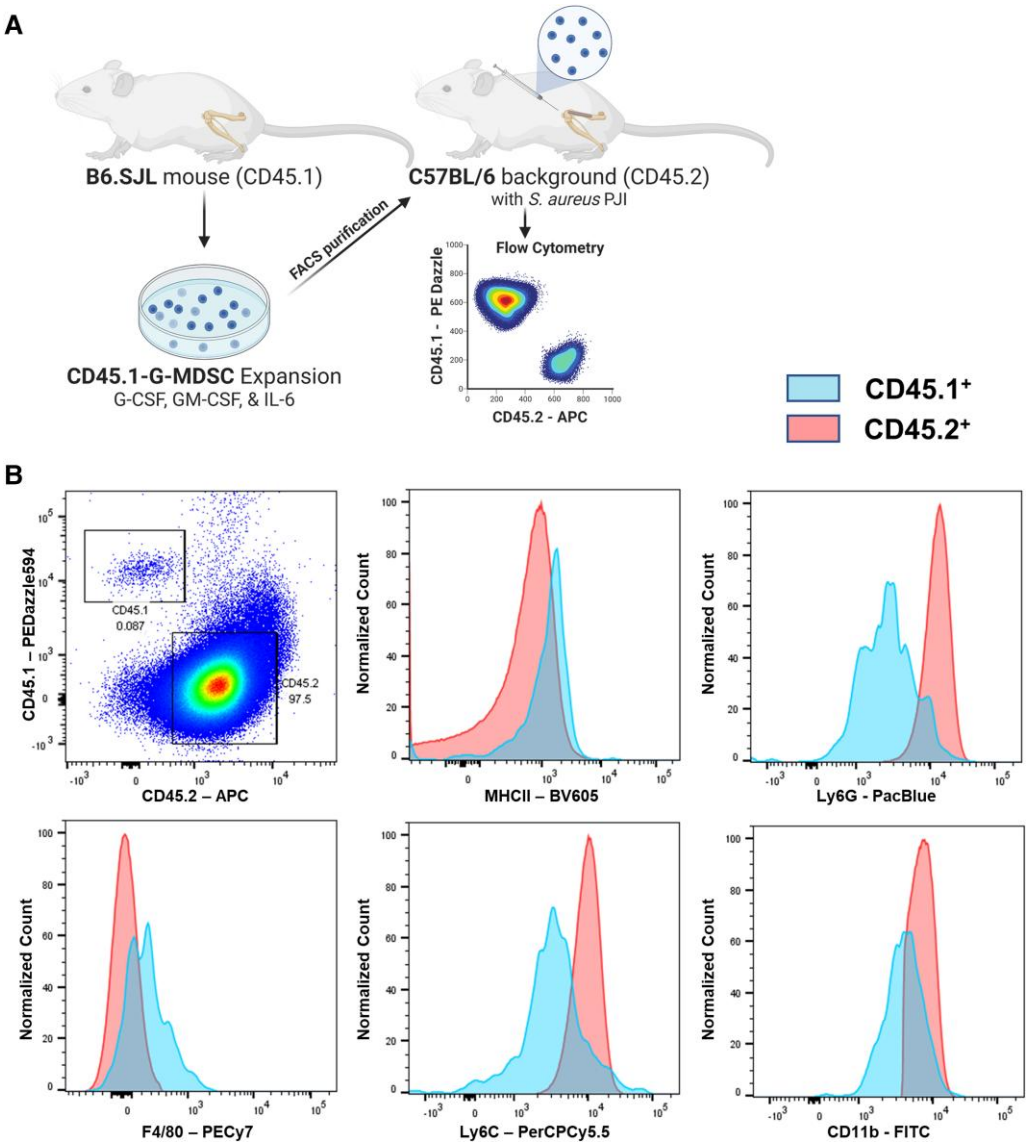

Fig. 9. G-MDSCs acquire F4/80 and MHC class II expression within the biofilm milieu during *S. aureus* PJI. (A) Schematic representing the adoptive transfer workflow. CD45.1$^+$ G-MDSCs were expanded in vitro from the bone marrow of naive B6.SJL congenic mice, whereupon Ly6G$^+$Ly6C$^+$CD11b^{high}F4/80$^-$MHCII$^-$ cells were purified by FACS and injected into the knee tissue of IL-10 KO mice (CD45.2$^+$) at day 14 following *S. aureus* PJI. After 24 h, mice were euthanized, and the implant-associated tissue was analyzed using flow cytometry to compare CD45.1$^+$ transferred cells to endogenous CD45.2$^+$ G-MDSCs. (B) Dot plot and histograms are concatenated from 5 mice and are representative of 3 independent experiments.

providing further evidence of their unique immune characteristics. Our data suggest that a subpopulation of G-MDSCs within the infection milieu may acquire cell surface markers indicative of maturation, such as F4/80 and MHCII, but retain their immunosuppressive characteristics. This highlights the need for functional characterization of cells rather than solely relying on cell surface marker expression to infer activity.

To assess whether G-MDSCs exhibit plasticity at the site of *S. aureus* PJI, we used an adoptive transfer approach to monitor how cells adapt within the biofilm microenvironment. While most infiltrating leukocytes during PJI are G-MDSCs, single-point-in-time analyses like flow cytometry cannot discern whether this results from continued G-MDSC recruitment, the death of terminal effector cells, impaired differentiation, or any combination of these—all of which can serve to maintain a constant number of G-MDSCs at the site of infection. In our adoptive transfer experiments, only a small number of transferred G-MDSCs could be recovered after a 24-h period. This could result from a number of factors, including the short half-life of G-MDSCs,[13,46] killing by *S. aureus* toxins,[47] or trafficking of donor G-MDSCs away from the site of infection. The latter possibility appears unlikely since IVIS revealed that adoptively transferred G-MDSCs were retained at the infection site. Because of limitations with the number of G-MDSCs that could be generated in vitro at one time for adoptive transfers, we were not able to increase the number of transferred G-MDSCs to improve the frequency of detecting F480$^+$MHCII$^+$ MDSCs at 24 h postinfection. Nevertheless, these adoptive transfer experiments establish that G-MDSCs can acquire monocyte markers in vivo, which was the main objective of our studies and is difficult to assess with endogenous cell populations. Since G-MDSCs represent approximately 70% of the leukocyte infiltrate during PJI[10,23] and we show that these cells have the capacity to acquire F480$^+$MHCII$^+$ expression and are also highly suppressive, this suggests that they may cooperate

with traditional G-MDSCs to prevent *S. aureus* biofilm clearance. In addition, this study and our prior publications have reported the presence of G-MDSCs that also express F4/80, which constitute a smaller but consistent infiltrate during *S. aureus* biofilm infection.[12,35] Our studies advance these findings to demonstrate that the F480$^+$MHCII$^+$ MDSCs identified here may reflect these cells, and it is important to note that even a small number of cells with potent suppressive activity can exert meaningful biological effects. Nonetheless, the few CD45.1$^+$ G-MDSCs that were recovered acquired F4/80 and MHCII expression, suggesting G-MDSC phenotypic plasticity within the biofilm milieu.

There are a few limitations to this study. First, we utilized an adoptive transfer paradigm with B6.SJL congenic mice that express CD45.1 to discriminate between adoptively transferred and endogenous leukocytes.[33] Although this approach has been widely used, B6.SJL mice have recently been reported to harbor SJL genetic content that could affect immune cell activity.[34] However, this possibility is less likely given the finding that residual SJL mutations have been implicated in CD8 T-cell effector function and antiviral immunity, which are not applicable here based on the lack of T-cell infiltrates during PJI that is caused by a bacterial pathogen.[28,35] Second, our CITE-seq study examined only G-MDSC phenotypes at a single interval following *S. aureus* PJI (i.e. day 14). It would be interesting to extend this analysis to intervals on the spectrum of planktonic growth (day 3) to biofilm establishment (day 7) to compare with the day 14 interval reported here that reflects biofilm persistence.[24] Finally, it would be interesting to examine whether F4/80$^+$MHCII$^+$ MDSCs are present in human PJI tissues, since this population can be detected by flow cytometry. To date, our results have revealed a high degree of conservation in leukocyte infiltrates between human PJI tissues and our mouse model,[9,10,28,35,48] suggesting that F4/80$^+$MHCII$^+$ MDSCs may be present during human infection. This would be an interesting avenue for future exploration leveraging the CITE-seq platform to interrogate the transcriptional profile of this population.

Collectively, this study identifies a previously unknown population of G-MDSCs that acquire F4/80 and MHCII expression during *S. aureus* PJI. These cells exhibit immunosuppressive properties and increased TNF and IL-6 production. Future studies should be performed to determine if F4/80$^+$MHCII$^+$ MDSCs are present in other pathologies and the contribution of these cells to the inflammatory milieu.

Acknowledgments

The authors thank Rachel Fallet for managing the mouse colony and Zachary Van Roy for assistance with figures. This work was supported by the National Institutes of Health/National Institute of Allergy and Infectious Disease grant P01AI083211 (Project 4 to T.K.) and an American Heart Association Predoctoral Fellowship 831295 (to B.P.B.). The UNMC DNA Sequencing Core receives partial support from the National Institute for General Medical Science (NIGMS; INBRE—P20GM103427-14 and COBRE—1P30GM110768-01). Both the UNMC DNA Sequencing and Flow Cytometry Research Cores receive support from The Fred & Pamela Buffett Cancer Center Support Grant (P30CA036727).

Author contributions

B.P.B., C.E.H., and T.K. designed experiments. B.P.B., C.E.H., and S.A.K. conducted experiments. B.P.B. wrote the manuscript, and all authors edited and approved the final manuscript.

Supplementary material

Supplementary materials are available at *Journal of Leukocyte Biology* online.

Conflict of interest

The authors have no conflict of interest to report.

References

1. Veglia F, Sanseviero E, Gabrilovich DI. Myeloid-derived suppressor cells in the era of increasing myeloid cell diversity. *Nat Rev Immunol*. 2021:21(8):485–498. https://doi.org/10.1038/s41577-020-00490-y
2. Condamine T, Mastio J, Gabrilovich DI. Transcriptional regulation of myeloid-derived suppressor cells. *J Leukoc Biol*. 2015:98(6):913–922. https://doi.org/10.1189/jlb.4RI0515-204R
3. Bronte V, Brandau S, Chen S-H, Colombo MP, Frey AB, Greten TF, Mandruzzato S, Murray PJ, Ochoa A, Ostrand-Rosenberg S, *et al.* Recommendations for myeloid-derived suppressor cell nomenclature and characterization standards. *Nat Commun*. 2016:7(1):12150. https://doi.org/10.1038/ncomms12150
4. Dorhoi A, Glaría E, Garcia-Tellez T, Nieuwenhuizen NE, Zelinskyy G, Favier B, Singh A, Ehrchen J, Gujer C, Münz C, *et al.* MDSCs in infectious diseases: regulation, roles, and readjustment. *Cancer Immunol Immunother*. 2019:68(4):673–685. https://doi.org/10.1007/s00262-018-2277-y
5. Medina E, Hartl D. Myeloid-derived suppressor cells in infection: a general overview. *J Innate Immun*. 2018:10(5-6):407–413. https://doi.org/10.1159/000489830
6. Condamine T, Ramachandran I, Youn JI, Gabrilovich DI. Regulation of tumor metastasis by myeloid-derived suppressor cells. *Annu Rev Med*. 2015:66(1):97–110. https://doi.org/10.1146/annurev-med-051013-052304
7. Greten TF, Manns MP, Korangy F. Myeloid derived suppressor cells in human diseases. *Int Immunopharmacol*. 2011:11(7):802–807. https://doi.org/10.1016/j.intimp.2011.01.003
8. Gabrilovich DI. Myeloid-derived suppressor cells. *Cancer Immunol Res*. 2017:5(1):3–8. https://doi.org/10.1158/2326-6066.CIR-16-0297
9. Heim CE, Vidlak D, Scherr TD, Kozel JA, Holzapfel M, Muirhead DE, Kielian T. Myeloid-derived suppressor cells contribute to Staphylococcus aureus orthopedic biofilm infection. *J Immunol*. 2014:192(8):3778–3792. https://doi.org/10.4049/jimmunol.1303408
10. Heim CE, West SC, Ali H, Kielian T. Heterogeneity of Ly6G(+) Ly6C(+) myeloid-derived suppressor cell infiltrates during Staphylococcus aureus biofilm infection. *Infect Immun*. 2018:86(12):e00684–18. https://doi.org/10.1128/IAI.00684-18
11. Heim CE, Vidlak D, Kielian T. Interleukin-10 production by myeloid-derived suppressor cells contributes to bacterial persistence during Staphylococcus aureus orthopedic biofilm infection. *J Leukoc Biol*. 2015:98(6):1003–1013. https://doi.org/10.1189/jlb.4VMA0315-125RR
12. Aldrich AL, Horn CM, Heim CE, Korshoj LE, Kielian T. Transcriptional diversity and niche-specific distribution of leukocyte populations during *Staphylococcus aureus* craniotomy-associated biofilm infection. *J Immunol*. 2020:206(4):751–765. https://doi.org/10.4049/jimmunol.2001042
13. Condamine T, Kumar V, Ramachandran IR, Youn JI, Celis E, Finnberg N, El-Deiry WS, Winograd R, Vonderheide RH, English NR, *et al.* ER stress regulates myeloid-derived suppressor cell fate through TRAIL-R-mediated apoptosis. *J Clin Invest*. 2014:124(6):2626–2639. https://doi.org/10.1172/JCI74056

14. Corzo CA, Condamine T, Lu L, Cotter MJ, Youn JI, Cheng P, Cho HI, Celis E, Quiceno DG, Padhya T, *et al.* HIF-1α regulates function and differentiation of myeloid-derived suppressor cells in the tumor microenvironment. *J Exp Med*. 2010:207(11):2439–2453. https://doi.org/10.1084/jem.20100587
15. Narita Y, Wakita D, Ohkur T, Chamoto K, Nishimura T. Potential differentiation of tumor bearing mouse CD11b+Gr-1+ immature myeloid cells into both suppressor macrophages and immunostimulatory dendritic cells. *Biomed Res*. 2009:30(1):7–15. https://doi.org/10.2220/biomedres.30.7
16. Nefedova Y, Nagaraj S, Rosenbauer A, Muro-Cacho C, Sebti SM, Gabrilovich DI. Regulation of dendritic cell differentiation and antitumor immune response in cancer by pharmacologic-selective inhibition of the janus-activated kinase 2/signal transducers and activators of transcription 3 pathway. *Cancer Res*. 2005:65(20):9525–9535. https://doi.org/10.1158/0008-5472.CAN-05-0529
17. Zhong H, Gutkin DW, Han B, Ma Y, Keskinov AA, Shurin MR, Shurin GV. Origin and pharmacological modulation of tumor-associated regulatory dendritic cells. *Int J Cancer*. 2014:134(11):2633–2645. https://doi.org/10.1002/ijc.28590
18. Mastio J, Condamine T, Dominguez G, Kossenkov AV, Donthireddy L, Veglia F, Lin C, Wang F, Fu S, Zhou J, *et al.* Identification of monocyte-like precursors of granulocytes in cancer as a mechanism for accumulation of PMN-MDSCs. *J Exp Med*. 2019:216(9):2150–2169. https://doi.org/10.1084/jem.20181952
19. Greten FR, Grivennikov SI. Inflammation and cancer: triggers, mechanisms, and consequences. *Immunity*. 2019:51(1):27–41. https://doi.org/10.1016/j.immuni.2019.06.025
20. Draghiciu O, Lubbers J, Nijman HW, Daemen T. Myeloid derived suppressor cells-an overview of combat strategies to increase immunotherapy efficacy. *Oncoimmunology*. 2015:4(1):e954829. https://doi.org/10.4161/21624011.2014.954829
21. Voyich JM, Braughton KR, Sturdevant DE, Whitney AR, Saïd-Salim B, Porcella SF, Long RD, Dorward DW, Gardner DJ, Kreiswirth BN, *et al.* 2005. Insights into mechanisms used by staphylococcus aureus to avoid destruction by human neutrophils. *J Immunol* 175:3907–3919. https://doi.org/10.4049/jimmunol.175.6.3907.
22. Diep BA, Palazzolo-Ballance AM, Tattevin P, Basuino L, Braughton KR, Whitney AR, Chen L, Kreiswirth BN, Otto M, DeLeo FR, *et al.* Contribution of Panton-Valentine leukocidin in community-associated methicillin-resistant Staphylococcus aureus pathogenesis. *PLoS One*. 2008:3(9):e3198. https://doi.org/10.1371/journal.pone.0003198
23. Heim CE, Bosch ME, Yamada KJ, Aldrich AL, Chaudhari SS, Klinkebiel D, Gries CM, Alqarzaee AA, Li Y, Thomas VC, *et al.* Lactate production by Staphylococcus aureus biofilm inhibits HDAC11 to reprogramme the host immune response during persistent infection. *Nat Microbiol*. 2020:5(10):1271–1284. https://doi.org/10.1038/s41564-020-0756-3
24. Yamada KJ, Heim CE, Xi X, Attri KS, Wang D, Zhang W, Singh PK, Bronich TK, Kielian T. Monocyte metabolic reprogramming promotes pro-inflammatory activity and Staphylococcus aureus biofilm clearance. *PLoS Pathog*. 2020:16(3):e1008354. https://doi.org/10.1371/journal.ppat.1008354
25. Stoeckius M, Hafemeister C, Stephenson W, Houck-Loomis B, Chattopadhyay PK, Swerdlow H, Satija R, Smibert P. Simultaneous epitope and transcriptome measurement in single cells. *Nat Methods*. 2017:14(9):865–868. https://doi.org/10.1038/nmeth.4380
26. Stoeckius M, Zheng S, Houck-Loomis B, Hao S, Yeung BZ, Mauck WM III, Smibert P, Satija R. Cell hashing with barcoded antibodies enables multiplexing and doublet detection for single cell genomics. *Genome Biol*. 2018:19(1):224. https://doi.org/10.1186/s13059-018-1603-1
27. Aran D, Looney AP, Liu L, Wu E, Fong V, Hsu A, Chak S, Naikawadi RP, Wolters PJ, Abate AR, *et al.* Reference-based analysis of lung single-cell sequencing reveals a transitional profibrotic macrophage. *Nat Immunol*. 2019:20(2):163–172. https://doi.org/10.1038/s41590-018-0276-y
28. Heim CE, Vidlak D, Odvody J, Hartman CW, Garvin KL, Kielian T. Human prosthetic joint infections are associated with myeloid-derived suppressor cells (MDSCs): implications for infection persistence. *J Orthop Res*. 2018:36(6):1605–1613. https://doi.org/10.1002/jor.23806
29. Austyn JM, Gordon S. F4/80, a monoclonal antibody directed specifically against the mouse macrophage. *Eur J Immunol*. 1981:11(10):805–815. https://doi.org/10.1002/eji.1830111013
30. Li J, Zhang Y, Yang C, Rong R. Discrepant mRNA and protein expression in immune cells. *Curr Genomics*. 2020:21(8):560–563. https://doi.org/10.2174/1389202921999200716103758
31. Menousek J, Horn CM, Heim CE, Van Roy Z, Korshoj LE, Kielian T. Transcriptional profiling of phagocytic leukocytes and microglia reveals a critical role for reactive oxygen species in biofilm containment during staphylococcus aureus craniotomy infection. *J Immunol*. 2022:209(10):1973–1986. https://doi.org/10.4049/jimmunol.2200503
32. Alshetaiwi H, Pervolarakis N, McIntyre LL, Ma D, Nguyen Q, Rath JA, Nee K, Hernandez G, Evans K, Torosian L, *et al.* Defining the emergence of myeloid-derived suppressor cells in breast cancer using single-cell transcriptomics. *Sci Immunol*. 2020:5(44):eaay6017. https://doi.org/10.1126/sciimmunol.aay6017
33. Shen FW, Saga Y, Litman G, Freeman G, Tung JS, Cantor H, Boyse EA. Cloning of Ly-5 cDNA. *Proc Natl Acad Sci U S A*. 1985:82(21):7360–7363. https://doi.org/10.1073/pnas.82.21.7360
34. Chisolm DA, Cheng W, Colburn SA, Silva-Sanchez A, Meza-Perez S, Randall TD, Weinmann AS. Defining genetic variation in widely used congenic and backcrossed mouse models reveals varied regulation of genes important for immune responses. *Immunity*. 2019:51(1):155–168.e5. https://doi.org/10.1016/j.immuni.2019.05.006
35. Heim CE, Vidlak D, Scherr TD, Hartman CW, Garvin KL, Kielian T. IL-12 promotes myeloid-derived suppressor cell recruitment and bacterial persistence during Staphylococcus aureus orthopedic implant infection. *J Immunol*. 2015:194(8):3861–3872. https://doi.org/10.4049/jimmunol.1402689
36. Feil S, Krauss J, Thunemann M, Feil R. Genetic inducible fate mapping in adult mice using tamoxifen-dependent cre recombinases. *Methods Mol Biol*. 2014:1194:113–139. https://doi.org/10.1007/978-1-4939-1215-5_6
37. Scherr TD, Hanke ML, Huang O, James DB, Horswill AR, Bayles KW, Fey PD, Torres VJ, Kielian T. Staphylococcus aureus biofilms induce macrophage dysfunction through leukocidin AB and alpha-toxin. *mBio*. 2015:6(4):e01021–e01015. https://doi.org/10.1128/mBio.01021-15
38. Tam K, Torres VJ. Staphylococcus aureus secreted toxins and extracellular enzymes. *Microbiol Spectr*. 2019:7(2):10.1128/microbiolspec.GPP3-0039-2018. https://doi.org/10.1128/microbiolspec.GPP3-0039-2018
39. Kumar V, Cheng P, Condamine T, Mony S, Languino LR, McCaffrey JC, Hockstein N, Guarino M, Masters G, Penman E, *et al.* CD45 phosphatase inhibits STAT3 transcription factor activity in myeloid cells and promotes tumor-associated macrophage differentiation. *Immunity*. 2016:44(2):303–315. https://doi.org/10.1016/j.immuni.2016.01.014

40. Youn JI, Kumar V, Collazo M, Nefedova Y, Condamine T, Cheng P, Villagra A, Antonia S, McCaffrey JC, Fishman M, *et al*. Epigenetic silencing of retinoblastoma gene regulates pathologic differentiation of myeloid cells in cancer. *Nat Immunol*. 2013:14(3):211–220. https://doi.org/10.1038/ni.2526
41. Sato Y, Shimizu K, Shinga J, Hidaka M, Kawano F, Kakimi K, Yamasaki S, Asakura M, Fujii S-i. Characterization of the myeloid-derived suppressor cell subset regulated by NK cells in malignant lymphoma. *OncoImmunology*. 2015:4(3):e995541. https://doi.org/10.1080/2162402X.2014.995541
42. Schröder M, Krötschel M, Conrad L, Naumann SK, Bachran C, Rolfe A, Umansky V, Helming L, Swee LK. Genetic screen in myeloid cells identifies TNF-α autocrine secretion as a factor increasing MDSC suppressive activity via nos2 up-regulation. *Sci Rep*. 2018:8(1):13399. https://doi.org/10.1038/s41598-018-31674-1
43. Sade-Feldman M, Kanterman J, Ish-Shalom E, Elnekave M, Horwitz E, Baniyash M. Tumor necrosis factor-alpha blocks differentiation and enhances suppressive activity of immature myeloid cells during chronic inflammation. *Immunity*. 2013:38(3):541–554. https://doi.org/10.1016/j.immuni.2013.02.007
44. Condamine T, Gabrilovich DI. Molecular mechanisms regulating myeloid-derived suppressor cell differentiation and function. *Trends Immunol*. 2011:32(1):19–25. https://doi.org/10.1016/j.it.2010.10.002
45. Zhao X, Rong L, Zhao X, Li X, Liu X, Deng J, Wu H, Xu X, Erben U, Wu P, *et al*. TNF signaling drives myeloid-derived suppressor cell accumulation. *J Clin Invest*. 2012:122(11):4094–4104. https://doi.org/10.1172/JCI64115
46. Sinha P, Chornoguz O, Clements VK, Artemenko KA, Zubarev RA, Ostrand-Rosenberg S. Myeloid-derived suppressor cells express the death receptor Fas and apoptose in response to T cell-expressed FasL. *Blood*. 2011:117(20):5381–5390. https://doi.org/10.1182/blood-2010-11-321752
47. Seilie ES, Bubeck Wardenburg J. Staphylococcus aureus pore-forming toxins: the interface of pathogen and host complexity. *Semin Cell Dev Biol*. 2017:72:101–116. https://doi.org/10.1016/j.semcdb.2017.04.003
48. Bertrand BP, Heim CE, West SC, Chaudhari SS, Ali H, Thomas VC, Kielian T. Role of staphylococcus aureus formate metabolism during prosthetic joint infection. *Infect Immun*. 2022:90(11):e0042822. https://doi.org/10.1128/iai.00428-22